International Journal of Chemistry Studies
www.chemistryjournal.in
ISSN: 2581-348X
Impact Factor: RJIF 5.44
Volume 2; Issue 3; May 2018; Page No. 10-16

Palladium supported on titanium oxide nanoparticles as a catalyst for methanol oxidation reaction

Nabil AN Alkadasi[1*], MA Awad[2], MA Ghanem[3], AM Al-Mayouf[4]

[1, 2] Department of Chemistry, Faculty of Applied Science, Thamar University, Thamar, Yemen.

[1] Department of Chemistry, Faculty of Engineering, Thamar University, Thamar, Yemen

[2, 3, 4] Department of Chemistry, College of Science, King Saud University, Riyadh 11451, Saudi Arabia

[3] Department of Science & Math, Faculty of Petroleum & Mining Engineering, Suez University, Suez, Egypt

Abstract
In this work, TONPs powder (titanium oxide nanoparticles powder)prepared by anodization in 0.7 M $HClO_4$ was annealed in N_2 at 450°C for 3 h to obtain the TONPs-N_2 powder as catalyst support to which Pd was loaded by photodeposition technique using $PdCl_2$ and isopropanol as sacrificial donor. The resulting Pd-TONPs-N_2 powder catalyst exhibited high surface area of 98m^2/g. The physicochemical characterization of TONPs arrays powder were performed by X-ray diffraction (XRD), scanning electron microscopy (SEM), transmission electron microscopy (TEM), energy dispersive x-ray (EDX), and surface area and pore size analysis. The catalyst support TONPs arrays powder were electrochemically characterized in basic solution of methanol by cyclic voltammetry (CV), and chronoamperometry measurements. Pd-TONPs-N_2 powder electrode catalyst exhibited a remarkably high electrocatalytic activity and has high electrocatalytic stability for methanol electrocatalytic oxidation reaction. Pd supported on the conductive support TONPs-N_2 is used as electrocatalyst in fuel cells.

Keywords: methanol oxidation, titanium oxide nanoparticles powder, photo deposition, Pd electro catalyst, chronoamperometry

1. Introduction
In recent times, a great deal attention has been paid to the electrochemical oxidation of small organic molecules for fuel cells application [1, 2]. Compared to other small organic molecules and especially to methanol, ethanol has been used more extensively as an alternative fuel in direct alcohol fuel cells since it is less toxic and has low volatility together with a higher energy density (8.01kWh/kg versus 6.09kWh/kg). It can easily be formed in huge quantities by the fermentation of sugar containing raw materials and biomass [3-6]. On the other hand, the electrochemical reactivity of ethanol is slightly lower than that of methanol. Partial oxidation of ethanol can lead to the formation of acetaldehyde, acetic acid, or carbon monoxide, which can be easily adsorbed on the electrode surface and decrease its catalytic activity towards ethanol oxidation [7-13]. Therefore, many new kinds of catalysts have been developed toward ethanol oxidation at low potentials, such as Pd, Pt, and Au, and their metallic nanoparticles [14–17] and alloys [18–20] prepared with other transition metals, which have higher electrocatalytic activity toward the oxidation of ethanol. Direct alcohol fuel cells (DAFCs) generate electricpower by feeding liquid fuels directly to anode, whichmakes them easier to design small and lightweight powersources. DAFCs are promising power sources for portable electronic devices and electric vehicles [21, 22].
Pt and Pt-based catalysts have been extensively investigated as the electrocatalysts for the oxidation of liquid fuels such as methanol and ethanol [25–28]. However, the high price and limited supply of Pt constitute a major barrier to the development of DAFCs. Our previous work on the development of Pt-free electrocatalysts for alcohol oxidation has focused on Pd electrocatalysts [29–32]. The results revealed that Pd is a good electrocatalyst for methanol oxidation in alkaline media and shows higher activity and better steady-state behaviour than Pt. A unique tolerance of Pd surface against CO poisoning was observed in several studies [33–36]. The usage of Pd is interesting as it is at least fifty times abundant on the earth than Pt. Although Pd exhibits a high activity for methanol oxidation in alkaline media, a little information is devoted to the kinetics for methanol oxidation on Pd. Here, titanium supported Pd nanoparticles were fabricated by photodeposition method and used as the catalysts for methanol oxidation with varying the concentration of KOH and methanol. It is well known that the photodeposition is one of the most efficient methods for the growth of metal nanoparticles [37–40]. This is a powerful technique for the deposition of many metals since it is rapid and facile, allowing easy control of the nucleation and growth of metal nanoparticles with differing sizes,shapes and distributions [41]. The Pd nanoparticles arrays have been successfully prepared by photodeposition method [31, 42]. A titanium oxide nanoparticles (TONPs) were used as the substrate due to its excellent chemical stability. It is well know that titanium-supported catalysts present significant electrocatalytic activity for methanol oxidation [43, 44]. TONPs-N_2 anodes prepared by photodeposition of the Pd directly on the surface have been used in direct methanol fuel cells (DMFCs) and show a higher performance than carbon black supported platinum anodes [45,46].

2. Experimental
2.1 Materials
Ti foils (>99.5% purity, Alfa Aesar, thickness: 0.25 mm), perchloric acid $HClO_4$Palladium (II) chloride ($PdCl_2$, Sigma–

Aldrich, 99.9+ %) as precursor, isopropanol (99.0 %) as sacrificial donor, TONPs powder (surface area 109m²/g).

2.2 Synthesis of Pd-TONPs-N_2 powder:

At the beginning titanium oxide nanoparticles powder (TONPs powder) was prepared bythe electrochemical anodic oxidation (annodization process). The Ti foils (>99.5% purity, Alfa Aesar, thickness: 0.25 mm) were anodized in an aqueous solution containing0.7 M perchloric acid $HClO_4$ using a two-electrode electrochemical cell (Ti foil as the anode and Pt foil as the cathode) at 20V for 1h at room temperature then, we separate the precipitate (TONPs powder) from the mixed solution using centrifuge. Then dry the precipitate in oven at 80 °C for overnight, then use pestle and mortar to make smooth powder to obtain TONPs powder. The TONPs powders were subsequently annealed at 450 °C in N_2 for 3hs with heating and cooling rates of 5 °C min^{-1} to obtain TONPs-N_2 powder.

Photodeposition by UV-400W lamp was carried out in an aqueous solution contains 150 mg of TiO_2 NPs powder, 10 ml of 20 mM $PdCl_2$, 10 ml of 0.3 M isopropanoland put in the beaker magnetic stirrer for 2hs. In this step we note change in the colour of the solution in the case of palladium from the yellow colour to the light green colour and this evidence that palladium is deposited on the surface of TONPs-N_2 powder.Then, we separate the precipitate (e.g. Pd adsorbed on TONPs-N_2 powder) from the mixed solution using centrifuge. Then dry the precipitate in oven at 80 °C for overnight, then use pestle and mortar to make smooth powder. Then to prepare the ink; weigh 50 mg of (Pd-TONPs-N_2powder) and add to it 1ml DI water plus 20 μL of nafion(5 wt. %) solution to stick the catalyst on the Au working electrode. After that, we loaded 3 $\mu l\ of$ the catalyst (Pd-TONPs-N_2powder) by micropipette on 3 mm Au polycrystalline working electrode to carry out cyclic voltammetry (CV).

2.3 Physicochemical Characterizations

Transmission electron microscopy (TEM) images were obtained using a JEOL JEM-2100F electron microscope operating at 200 kV.

X-ray diffraction (XRD) data were collected on a Model RIGAKU MINIFLEX 100 X-ray diffract meter, operating at tube voltage 40 kV and tube current 15 mA, using Cu(Kα), intensity was 0-400 cps, range of 2^{θ}(deg) was 5-80 degree i.e. wide angle. For chilar, the water flow rate was 3.7 L/min, scan rate either 5 °/min or 2 °/min. Monochromator is used.

BET surface area and porosity measurements were carried out by N_2 adsorption at 77.3 K using Quantachrome instrument. We obtain the following results.

2.4. Electrochemical measurements

Cyclic Voltammetry (CV)

CV was performed in a conventional three-electrode single-compartment Pyrex glass cell using a computerized potentiostat/galvanostat (Autolab, FRA2, μAUTOLAB, TYPE III). The reference and auxiliary electrodes were SCE and pure Pt-foil, respectively. All potentials provided in the text are based on the SCE electrode only. A Pt wire auxiliary electrode and a saturated calomel reference electrode (SCE) were used. Also 3mm Au polycrystalline working electrode was used (with geometric surface 0.07 cm^2).The software program used in cyclic voltammetry measurements were NOVA 1.9. An evenly distributed suspension ink of catalyst was prepared by ultrasonic the mixture of 50 mg catalyst and 1 mL D.I water for 30 min, and 3 μL of the resultant suspension was laid on the surface of Au polycrystalline working electrode (3 mm diameter, 0.07 cm^2). After drying at 40 °C, 1 μL of Nafion (5 wt. %) solution was covered on the catalyst surface and allowed to dry again. Thus, the working electrode was obtained, and the specific loading of metal on the Au working electrode surface was about 0.0555 mg (55.5μg). Electrochemical tests were performed in 2 M KOH + different concentrations of methanol.

Chronoamperometry (CA) was carried out in different potentials i.e. at -0.35V,-0.3V, - 0.2V.

3. Results and discussion

3.1. Physicochemical characterization of Pd-TONPs-N_2 powder catalyst

The TEM images (Fig.1 and Fig.2) approve the formation of Pd-TONPs-N_2 powder catalyst without varying the original morphology of TONPs. It also further confirmations for the palladium particles size.

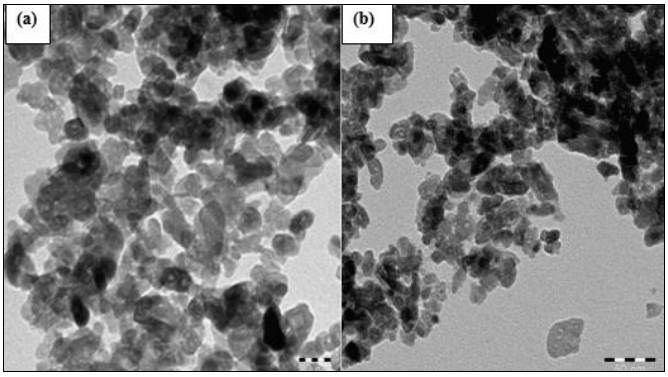

Fig 1: TEM (Transmission electron microscopy) image of TONPs powder annealed in nitrogen (a) 20 nm and (b) 50 nm.

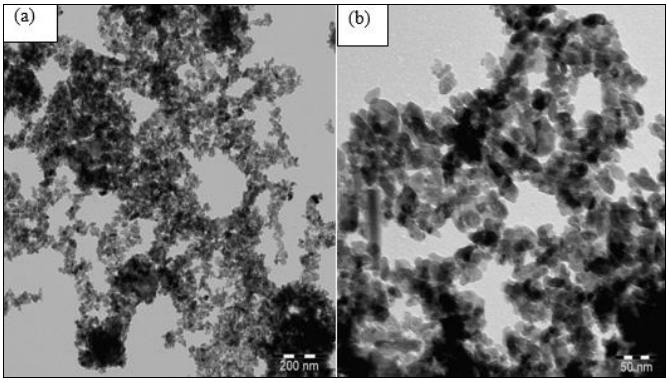

Fig. 2: (a) TEM image of Pd-TONPs-N_2 powder; (b) magnified image of Pd-TONPs-N_2 powder.

The X-ray diffraction shape of the prepared TONPs powder, TONPs-N_2 powder and Pd-TONPs-N_2 powder is revealed in Fig.3.Varshney *et al*. stated that nonappearance of unauthentic diffractions shows the crystallographic pureness [50]. The

experimental XRD patterns consistent with the XRD pattern of TONPs other literature [51]. Strong diffraction peaks at about 25° and 48° signifying TiO_2 in the anatase phase [52, 53]. It has been found that there is no any unauthentic diffraction peaks in the synthesized sample. The XRD peaks intensity of the TONPs reveals that the formed nanoparticles are crystalline and broad diffraction peaks point to very small size crystallite. The results confirmed the nanosized powder TONPs.

Pure anatase TiO_2 is detected in all samples signifying that its crystallinity is not affected via the photodeposition of palladium nanoparticles. The diffraction patterns of the synthesized anatase TiO_2 nanoparticles has the two most observable diffraction peaks detected at 2 θ equals to 25.3° (101) and 48.0° (200).The obtained pattern similarly verified the brookite and rutile phases presence. The occurrence of palladium nanoparticles is specified by diffraction peaks appeared at 2θ of 40.1 and 46.7°. They were ascribed to the (111) and (200) crystal plane spacings of face-centered cubic (FCC) palladium respectively [48]. From three peaks of palladium only two peaks were observed due to one peak overlaps with the anatase TiO_2 at 2θ = 68.1 (220).Hence, these diffraction peaks further indicate the metallic state for the loaded palladium nanoparticles [49]. Generally, the synthesized samples revealed high crystallinity which is confirmed by the sharp peaks obtained from all samples. The symbol A indicates to anatase and B indicates to titanium dioxide brookite, TiO_2.

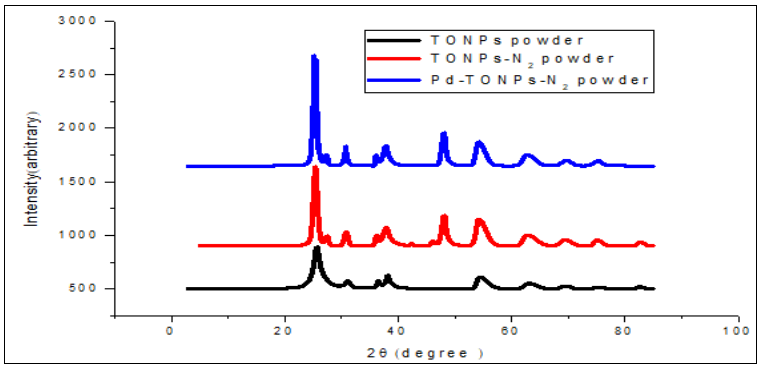

Fig 3: XRD pattern of TONPs powder, TONPs-N_2 powder and Pd-TONPs-N_2 powder.

Fig.4shows nitrogen adsorption-desorption isotherms of Pd-TONPs-N_2 powder expressed by relative pressure (P/P°) vs. cc/g (Volume @ STP) and their pore size distribution (b) i.e. (N_2-physiosorption isotherm and pore size distribution). It shows an obvious capillary condensation step of 0.6to 0.98 P/P°.

In Fig.4, all the samples have a step adsorption -desorption hysteresis, signified using isotherm is of type (IV), characteristic for TONPs materials with the features of a mesoporous material [54]. The differences in BET surface area, average pore size and pore volume after palladium adsorption is summarized in Table 3.6. Furthermore, the average pore diameter, measured through the Barrett-Joyner-Halenda (BJH) method by means of the adsorption isotherm (Fig.4b) was found to decrease after the adsorption of palladium nanoparticles. The decrease of BET surface area and average pore diameter was owing to a slight blocking of the pore in anatase TiO_2 via the photodeposited palladium nanoparticles [47].

The Pd-TONPs-N_2 powder catalyst possess a BET surface area of 98m^2/g and a total pore volume of 0.247cm^2/g. It has a bimodal pore size distribution with maxima about 2.0 and 2.9 nm (Fig. 4 b).

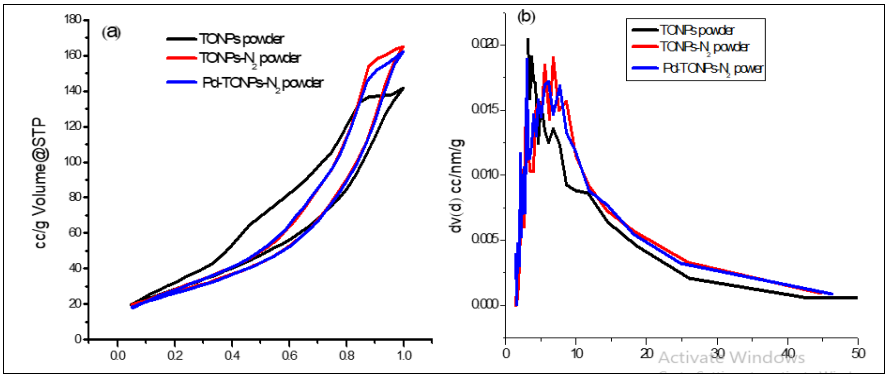

Fig 4: (a) Adsorption–desorption isotherm of TONPs powder, TONPs-N_2 powder and Pd-TONPs-N_2 powder (b) the average pore diameter, determined through the Barrett-Joyner-Halenda (BJH) method by the adsorption isotherm.

The results show that the mesoporous structure of TONPs-N_2 powder was maintained after loading of palladium. However, BET surface area of TONPs-N_2 powder was 99 m^2/g. The surface area of TONPs powder and Pd-TONPs-N_2 powder

were 109 and 98 m^2/g, respectively (Table 1). The decrease of surface area is mainly ascribed to the mesoporous of the support being partially covered or filled by palladium. Therefore, pore volume and average pore size also decrease from 0.249 cm^3/g to 0.247 cm^3/g, 6.80 nm to 2.952 nm. This indicates that Pd NPs was distributed evenly over the surface of TONPs-N_2 powder.

Table 1: The average BET surface area, average pore size and pore volume of TONPs, TONPs-N_2 and Pd-TONPs-N_2 powder.

	BET surface area (m^2/g)	Average pore size (Pore diameter) dv(d) (nm)	Pore volume in (cm^3/g)
TONPs powder	109	3.160	0.204
TONPs-N_2 powder	99	6.800	0.249
Pd-TONPs-N_2 powder	98	2.951	0.247

3.2 Methanol oxidation of Pd-TONPs-N_2 powder

Fig. 5 shows the electro catalytic activity of Pd-TONPs-N_2 powder used for methanol oxidation reaction i.e. show the CVs of the 3 µL Pd-TONPs-N_2 powder catalyst in 1 M methanol + 2 M KOH. It is clear that 1 M concentration of methanol gives high current density in contrast with other concentrations of methanol in basic medium of 2 M KOH.

Concerning the 1 M methanol concentration in basic medium, the peak current density in the forward scan for Pd-TONPs-N_2 powder catalyst were measured to be 21.3mA/cm^2 in alkaline medium whereas the peak current density in the backward scan were measured to be 7.4mA/cm^2.It is observed that the peak current is improved for catalyst prepared via photo deposition of $PdCl_2$ on TONPs-N_2 powder as support/catalyst using 0.3 M isopropanol.

Also the current of oxidation has been regularized to specific current density so as to the current density (I) can be directly used to differentiate between the catalytic activity of the samples. The Pd-TONPs-N_2 powder catalyst which was examined display a considerably enhanced methanol oxidation activity as compared to TONPs-N_2 powder catalyst support. The ratios of peak currents related to the anodic peaks in forward (I_f) and reverse (I_b) is largely used to describe the tolerance of a catalyst to intermediates engendered through the methanol oxidation [55].

A low I_f/I_b ratio points to poor electro oxidation of methanol to carbon dioxide CO_2 thru the forward scan, and too much accumulation of carbonaceous intermediates on the catalyst surface [56].

For Pd-TONPs-N_2 powder, the value of I_f/I_b was 2.88 which is larger than that reported for Pt/carbon (0.75) [57] i.e. it is about 3.84times higher than that stated for Pt/carbon (0.75) and is about 2.48 times higher than that stated for Pd/AC activated carbon [61]. Also, Pd-TONPs-N_2 powder I_f/I_b ratio is about 1.28 times higher than that stated for Pd/TiO_2 Nano belts and is about 3.16 times higher than that stated for Pd/TiO_2 nanobelts-C.

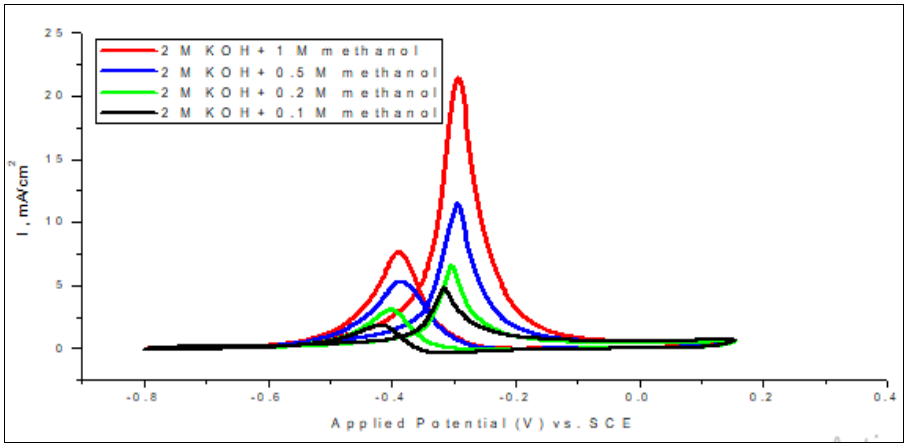

Fig 5: Effect of concentration of methanol on 3 µL Pd-TONPs-N_2 powder loaded on Au working electrode in 2 M KOH at a scan rate was 50mV/s by current density, scan was 50.

Table 2: The composition of the I_f/I_bratio for the 3µL catalysts loaded on Au polycrystalline working electrode at a scan rates was 50mV/s for (MOR).

Catalysts	I_f (mA/cm^2)	I_b (mA/cm^2)	Mass loading of Pd in (mg/ml)	I_f/I_b
Pd-TONPs-N_2 powder	21.3	7.4	0.0555 in 3 µL	2.88
Pt/C	0.75	1.0	……	0.75[57]
Pd/TiO_2 Nano belts	2.57	1.14	0.523 in 3 µL	2.25[61]
Pd/AC Activated carbon	2.9	2.5	0.353 in 3 µL	1.16[61]
Pd/TiO_2 nanobelts-C	4.0	4.4	0.3348 in 3 µL	0.91[61]

This enhancement in the catalytic activity cannot be ascribed only to the Pd NPs size but also due to the increased of Pd

(200) and Pd (220) surface sites that makes overlap with the anatase TONPs at 2θ = 68.1 (220). It is well recognized that the catalytic activity of palladium for methanol electrooxidation is sensitive to the structure of the palladium surface.

Fig. 6 displays the effect of the scan rate for methanol oxidation process at Pd-TONPs-N_2 powder catalyst in 2 M KOH in the existence of 1 M methanol. The curve displays that the anodic current for methanol oxidation at Pd-TONPs-N_2 powder catalyst increases speedily with increasing the potential scan rate and anodic potential shift toward higher potential values. Actually the time window for methanol oxidation process at higher scan rates turn into very narrow where facile electron transfer happens between methanol and catalytic sites. The proportionality of anodic peak currents to the scan rate in a range of 10-150 mV/s was illustrated in Fig.7. The anodic peak current are linearly proportional to the scan rate propose that the total oxidation of methanol at this electrode is organized via the methanol diffusion from solution to surface redox sites [58, 59].

Fig. 6 shows the scan rate effect for Pd-TONPs-N_2 powder electrode in a potential range from (-0.8 V to 0.15 V) recorded at different scan rate for 1 M methanol in basic medium (2 M KOH) solution, Fig. 6 shows an enhanced cathodic and anodic peak current that increase linearly with increasing scan rate, this performance is characteristic of an electrochemical reaction controlled by a diffusion process.

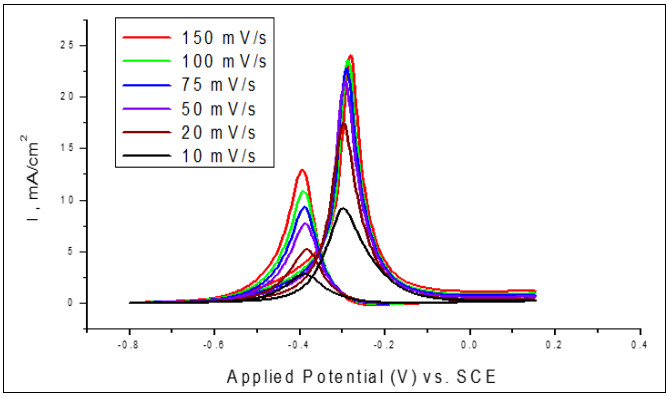

Fig 6: CV of Pd-TONPs-N_2 powder loaded on 3 mm diameter Au working electrode in (2M KOH+1M methanol), 3 microliter loading by current density, 50cycles (effect of scan rate).

It is more convenient and practical to evaluate the performance of materials for MOR according to spontaneous and apparent parameters, namely onset potential (E_{onset}) or the position of the forward anodic peak (E_f), forward anodic peak current density (E_f), and the ratio between the forward anodic peak current density to the backward anodic peak current density (I_f/I_b), which reflect the catalytic activity, the maximum performance, and the tolerance towards the adsorbed carbonaceous intermediates (s), respectively, of the electro catalyst.

Table 3: Scan rate (mV/s) and $\sqrt{\text{scan rate}}$ ($\sqrt{(mV/s)}$) vs. I_p (peak height –mA/cm^2) for both the forward and backward paths also contains the values of I_f/I_b for the Pd-TONPs-N_2 powder catalyst loaded on 3 mm Au polycrystalline working electrode 50 cycles for (MOR).

Scan rate (mV/s)	$\sqrt{scan rate}$ ($\sqrt{\frac{mV}{s}}$)	I_f (mA/cm^2)	I_b (mA /cm^2)	I_f/I_b
10	3.162	14.88	2.72	3.265
20	4.472	17.08	4.92	3.472
50	7.071	21.3	7.4	2.88
75	8.660	22.38	8.98	2.492
100	10	23.40	10.58	2.212
150	12.247	25.69	12.74	1.859

As we note from the Fig.7 that the forward direction or path is linear and this indicates that the forward is diffusion control. The backward direction is linear and this indicates that the backward is also diffusion control.

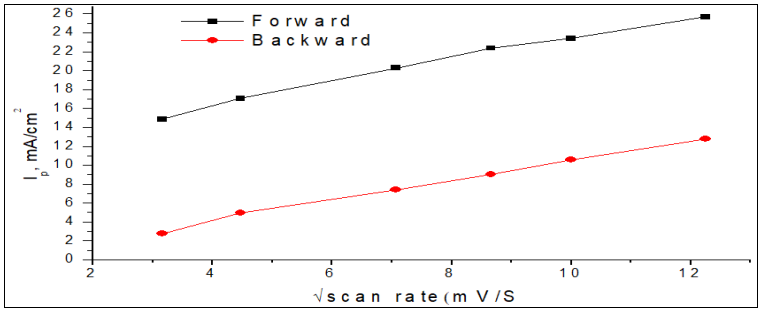

Fig 7: $\sqrt{\text{scan rate}}$ ($\sqrt{(mV/s)}$) vs. I_p (peak height - mA/cm^2) for both forward and backward paths.

Fig. 8 shows the catalytic stability of the Pd-TONPs-N_2 powder catalyst from first cycle to 50 cycles in (2 M KOH + 1 M methanol) with a scan rate was 50mV/s. Stability test was performed for Pd-TONPs-N_2 powder catalyst. Fig.8 shows the CVs for Pd-TONPs-N_2 powder catalyst after continuous cycling between -0.8 V and 0.15 V for a total of 50 cycles. The catalytic stability of Pd-TONPs-N_2 powder catalyst for methanol oxidation was characterized by means of CV as shown in Fig. 8. The Pd-TONPs-N_2 powder methanol oxidation current shows a steady decrease in current density

within the first few cycles (10 cycles) and then an approximately constant current density was gradually established for longer time. Therefore, the results reveal that Pd-TONPs-N_2 powder possesses high catalytic activity and stability in alkaline media.

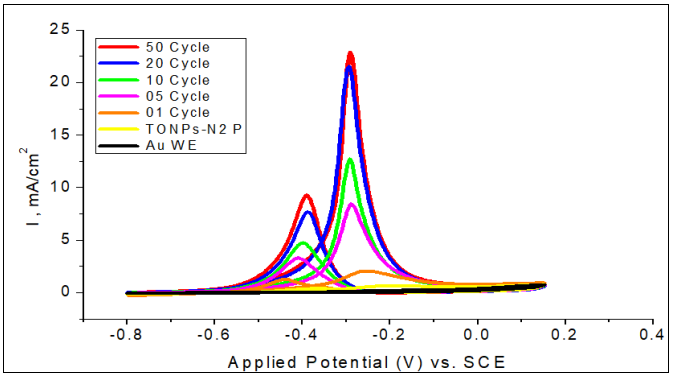

Fig 8: CV of Pd-TONPs-N_2 powder, catalyst loading 3 µL, 50 cycle, 20 cycle, 10 cycle, 5 cycle, 1cycle, 3μl TONPs-N_2 all was loaded on Au working electrode as baseline, also all in (2M KOH+1M methanol) at a scan rate was 50 mV/s by current density.

Fig.9 shows the CA for Pd-TONPs-N_2 powder loaded on 3 mm diameter Au working electrode in (2 M KOH+ 1M methanol) at different potentials (-0.35 V,-0.3 V and -0.2 V). At the principal step of the chronoamperometry (CA) curves, the current density is comparatively high owing to the methanol molecules adhesion on the active sites. Then the current density decrease through increasing time. Almost 200 s later, the curve becomes steady. It is well known that there are two probable causes for decreasing of catalyst activity with increasing time. First, the rate of intermediates desorption is slower than that of methanol oxidation, hence toxic intermediates would accumulate on the active sites. Second, catalyst nanoparticles commonly suffer from coarsening which result in disintegration of active sites through the catalytic process [60].

The stable current density of the Pd-TONPs-N_2 powder at the potential -0.35 V is the highest among the other potentials -0.3 V and -0.2 V, signifying that this would attain sense of balance among catalytic activity and poison resistance because of suitable deposition quantity of Pd nanoparticles on titanium oxide nanoparticles.

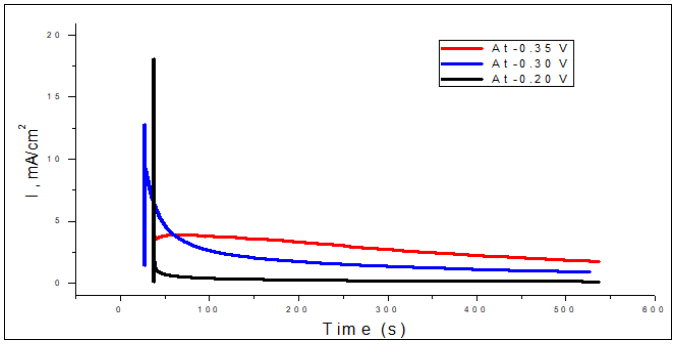

Fig 9: Chronoamperometry (CA) for Pd-TONPs-N_2 powder loaded on 3 mm diameter Au working electrode in (2 M KOH+ 1M methanol).

4. Conclusions

Integrating and enhance the palladium catalysts that has high electrochemical surface area into TONPs using photodeposition technique. The structure and electrochemical characterizations revealed that the TONPs conductivity was significantly enhanced by annealing in N_2 atmosphere and all incorporated catalysts had high catalytic activity for methanol oxidation reactions (MOR), demonstrated through an increase in current density, stability and better catalyst poisons tolerance.

5. Acknowledgements

The author would like to thank Professor Nabil Alkadasi for his non-stop guidance; support throughout the last two years.

6. References

1. Kuk ST, Wieckowski AJ. Power Sources. 2005; 141:1-7.
2. Arico AS, Baglio V, Di Blasi A, Modica E, Monforte G. Antonucci VJ. Electroanal. Chem. 2005; 576:161-169.
3. Lamy C, Belgsir EM, L´eger JMJ. Appl. Electrochem. 2001; 31:799-809.
4. Maillard F, Gloaguen F, Hahn F, L´eger JM. Fuel Cells 2002; 2:143-152.
5. Rousseau S, Coutanceau C, Lamy CL, eger JMJ. Power Sources. 2006; 158:18-24.
6. Wang J, Wasmus S, Savinell RFJ. Electrochem. Soc. 1995; 142:4218-4224.
7. Wang H, Jusys Z, Behm RJJ. Phys. Chem. B. 2004; 108, 19413-19424.
8. Tarnowski DJ, Korzeniewski CJ. Phys. Chem. B. 1997; 101:253-258.
9. Lamy C, Belgsir EM, L´eger JMJ. Appl. Electrochem. 2001; 31:799-809.
10. Vigier F, Coutanceau C, Perrard A, Belgsir EM, Lamy CJ. Appl. Electrochem. 2004; 34:439-446.
11. Mann J, Yao N, Bocarsly AB. Langmuir. 2006; 22:10432-10436.
12. Simoes FC, Dos Anjos DM, Vigier F, Leger JM, Hahn F, Coutanceau C, Power Sources. 2007; 167:1-10.
13. Wang H, Liu ZPJ. Phys. Chem. C. 2007; 111:12157-12160.
14. Bambagioni V, Bianchini C, Marchionni A, Filippi J, Vizza F, Teddy J, Serp P, Zhiani MJ. Power Sources. 2009; 190:241-251.
15. Zheng HT, Li Y, Chen S, Shen PKJ. Power Sources. 2006; 163:371-375.
16. He Q, Chen W, Mukerjeea S, Chen S, Laufek, F. J. Power Sources. 2009; 187:298-304.
17. Alvisi M, Galtieri G, Giorgi L, Giorgi R, Serra E, Signore MA. Surf. Coat. Tech. 2005; 200:1325-1329.
18. Godoi DRM, Perez J, Villullas HMJ. Power Sources. 2010; 195:3394-3401.
19. Colmenares L, Wang H, Jusys Z, Jiang L, Yan S, Sun GQ, Behm RJ. Electrochim. Acta. 2006; 52:221-233.
20. Chu D, Wang, J.; Wang, S.; Zha, L.; He, J.; Hou, Y, *et al*. Catal. Commun. 2009; 10:955-958.
21. Barraga VM, Heinzel A, Power Sources. 2002; 104:66.
22. Tang HL, Wang SL, Pan M, Jiang SP, Ruan YZ, Electrochim. Acta. 2007; 52:3714.

23. Song SQ, Tsiakaras P., Appl. Catal. B. 2006; 63:187.
24. Antolini E, Power Sources. 2007; 170:1.
25. Xu CW, Shen PK, Ji XZ, Zeng R, Liu YL. Electrochem. Commun. 2005; 7:1305.
26. Wei ZD, Li LL, Luo YH, Yan C, Sun CX, Yin GZ, Shen PK. J. Phys. Chem. B. 2006; 110:26055.
27. Chen SL. Schell M. Electrochim. Acta. 1999; 4:4773.
28. Chen SL, Schell M, Electroanal J Chem. 1999; 478:108.
29. Xu CW, Cheng LQ, Shen PK, Liu YL. Electrochem. Commun. 2007; 9:997.
30. Xu CW, Shen PK, Liu YL. J Power Sources164; 2007:527.
31. Wang H, Xu CW. Cheng FL. S.P. Jiang, Electrochem. Commun. 2007; 9:1212.
32. Shen PK. Xu CW. Electrochem. Commun. 2006; 8:84.
33. Capon A, Parsons R, Electroanal J Chem. 1973; 44:285.
34. Baldauf M, Kolb DM. J Phys. Chem. 1996; 100:11375.
35. Hara M, Linke U, Wandlowski T. Electrochim. Acta. 2007; 52:5733.
36. Hu FP, Chen CL, Wang JY, Wei GY, Shen PK. Electrochim. Acta. 2006; 52:1087.
37. Wei ZD, Chan SH. J Electroanal. Chem. 2004; 569:23.
38. Ordeig O, Banks CE, Campo FJ. Munoz FX/. J Davis, R.G. Compton, Electroanal. 2006; 18:247.
39. Ji XB, Banks CE, Holloway AF, Jurkschat K, Thorogood GG. Wildgoose RG. Compton, Electroanal. 2006; 18:2481.
40. Liu P, Guo XA, Huang H, Yang QQ, Tong YX, Hope GA, Adv. Mater. 2006; 18:1873.
41. Welch CM, Compton RJ. Anal. Biochem. 2006; 384:601.
42. Ji XB, Banks CE, Xi W, Wilkins SZ, Compton RJ. J Phys. Chem. B. 2006; 110:22307.
43. Freitas RJ, Santos MC, Oliveira RTS. Bulho RSO. es, E.C. Pereira, J Power Sources. 2006; 158:164.
44. Oliveira MB, Profeti LPR P. Olivi, Electrochem. Commun. 2005; 7:703.
45. Yu K. Scott, Electrochem. Commun. 2004; 6:361.
46. Yang CC, Chiu SJ, Chien WC. Power Sources. 2006; 162:21.
47. Pan X. Xu YJ. J Phys. Chem. C. 2013; 117:17996-18005.
48. Wang M, Guo D, Li J, H.-l J. Solid State Chem. 2005; 178:996-2000.
49. Chan CC, Chang CC, Hsu WC, Wang SK, Lin J. Chem. Eng J. 2009; 152:492-497.
50. Varshney R, Bhadauria S, Gaur MS. Adv.Mat.Lett. 2003; 1(3):232-237.
51. Antic Z, Krsmanovic RM, Nikolic MG, Cincovic MM, Mitric M, Polizzi S, Dramicanin MD. Mat. Chem. Phys. 2012; 135:1064-1069.
52. Ba-Abbad M, Kadhum AH, Mohamad A, Takriff MS VA, K. Sopian. Int. J. Electrochem. Sci. 2012; 7:4871-4888.
53. Thamaphat K, Limsuwan P, Ngotawornchai B. Kasetsart. J (Nat. Sci.). 2008; 42:357-361.
54. Pan X, Xu YJ. Appl. Catal. 459A, 2013, 34-40.
55. Wu YN, Liao SJ, Liang ZX, Yang LJ, Wang RF. *J* Power Sources.2009; 194:805-810.
56. Wu JJ, Tang HL, Wan ZH. Ma. Electrochim. Acta. 2009; 54:1473-1477.
57. Nukumizu K, Nunoshige J, Takata T, Kondo JN, Hara M. Chem. Lett. 2003; 32:196-197.
58. Allen J. Bard. John Wiley and Sons Inc, New York, L.R.F, 2001.
59. De Gromoboy TS, Shreir LL. Electrochim. Acta. 21;1996: 11:895-904.0
60. Meier JC, Galeano C, Katsounaros I, Topalov AA, Kostka A, Schueth F, Mayrhofer LJF. ACS Catalysis. 2012; 2:832-843.
61. Robert Liang, Anming Hu, John Persic, Y. Norman Zhou. Nanomicro Letters. 2013; 5:202.